

Article

Modeling and Simulation of Multipumping Photovoltaic Irrigation Systems

Javier R. Ledesma , Rita H. Almeida  and Luis Narvarte

Instituto de Energía Solar, Universidad Politécnica de Madrid, 28031 Madrid, Spain; luis.narvarte@upm.es
* Correspondence: javier.ledesma@upm.es (J.R.L.); rita.hogan@upm.es (R.H.A.); Tel.: +34-910673485 (J.R.L.)

Abstract: The growing market of large-power photovoltaic irrigation systems (PVISs)—made of systems with different and several motor pumps working in parallel—needs simulation tools capable to estimate their energy and water productivity. The objective of this paper is to present the simulation models developed for parallel multipump PVISs fed by a single PV generator. These models seek to maximize the instantaneous water flow rate according to the available PV power and were developed for the typical configurations of large-power irrigation facilities. The models present some advantages when compared with the current state of the art (in which a single motor pump connected to a $1/N$ fraction of the PV generator is simulated and the result is multiplied by N): in the case of negligible hydraulic friction losses, the use of the multipump model shows gains with respect to the state of the art; in the case of appreciable friction losses, the current state of the art overestimates the productivity of the systems. Then, the ability of these models to compare different multipump designs is shown: two groups of pumps working at variable frequencies show better performance than a group working at a variable frequency and a group at a nominal frequency—an 8% increase in the water pumped is seen.

Keywords: photovoltaic; PV irrigation systems; multipumping; variable frequency; water pumping



Citation: Ledesma, J.R.; Almeida, R.H.; Narvarte, L. Modeling and Simulation of Multipumping Photovoltaic Irrigation Systems. *Sustainability* **2022**, *14*, 9318. <https://doi.org/10.3390/su14159318>

Academic Editor: Mohammed Lofly

Received: 16 June 2022

Accepted: 22 July 2022

Published: 29 July 2022

Publisher's Note: MDPI stays neutral with regard to jurisdictional claims in published maps and institutional affiliations.



Copyright: © 2022 by the authors. Licensee MDPI, Basel, Switzerland. This article is an open access article distributed under the terms and conditions of the Creative Commons Attribution (CC BY) license (<https://creativecommons.org/licenses/by/4.0/>).

1. Introduction

Photovoltaic (PV) pumping is a mature technology that has a long history. The first systems date from the 1970s [1], and, since then, it has been widely disseminated in different PV pumping programs. Newkirk, according to [2], created a bibliography of the published material on PV water pumping systems and found seven publications about systems in the Soviet Union, two in France, one in Germany, and three in the USA. Those outside the USA had peak powers ranging from 300 Wp to 1 kWp, while for those in the USA, detailed information was only available for a 25 kWp system. Between 1979 and 1981, the United Nations Development Program, with the support of the World Bank and the Intermediate Technology Development Group, implemented a pilot project to test and evaluate PV pumping systems with powers ranging from 100 to 300 Wp used in small-scale irrigation systems in Mali, Philippines, and Sudan [3]. Between 1977 and 1990, around 200 systems were installed in Mali, with a total installed power of 220 kWp [4,5]. Following the experience in Mali, the Permanent Interstate Committee for Drought Control in Sahel countries, in cooperation with the European Commission, launched the Solar Regional Program in the early 1990s [6], which allowed the installation of 1040 systems, with a total PV power of 1.3 MWp [5,6].

These pumping systems have a relatively small power (<40 kWp), and their technical configuration consists of a PV generator, a frequency converter, and a standard centrifugal pump [7] (Figure 1). Normally there is a water pool where the motor pump raises the water. The motor pump works at a variable frequency that depends on the instantaneous PV power available.

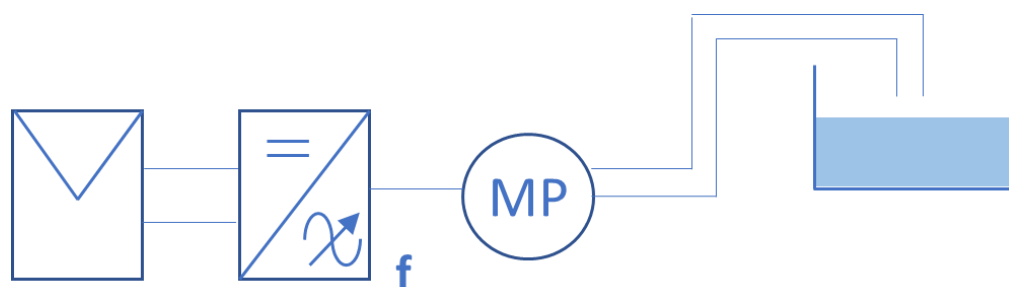


Figure 1. Configuration of a PV pumping system: PV generator, frequency converter, centrifugal motor pump, and water pool.

Despite being small systems, much research effort has been devoted to developing sizing methods and optimizing their design. For example, in [8], a simulation program was developed to determine the performance of a direct-coupled PV pumping system while in [9], a dynamic modeling tool was used to design a system by combining the models of the water demand, the solar PV power, and the pumping system. In [10], a methodology for the performance optimization of solar PV pumps based on the height of the water table and operating point of the pump using the most frequent conditions of a site was proposed. In [11], a differential evolution-based multiobjective optimization algorithm was proposed to optimally size a PV pumping system considering three weighted individual objectives—loss of load probability, life-cycle cost, and the volume of excess water. Considering some of these objectives, a new method based on the determination of loss of power supply probability was used in [12], a sizing model to optimize the sizes of the different components of a system with a water storage tank considering the loss of power supply probability and the life-cycle cost was recommended in [13], a technique for order performance by similarity to ideal solution method integrated with the analytic hierarchy process method was proposed to optimally size PV pumping systems based on the loss of load probability, the excess water volume, and the life-cycle cost [14]. Similarly, a techno-economic optimization model was recommended to determine optimally the capacity of the components of a system with a water storage tank (considering the deficiency of power supply probability and life-cycle costs) [15]. In [16], an approach to size the optimal surface of the photovoltaic modules, the optimal capacity of the battery bank, and the volume of the water storage tank was proposed. Finally, in [17], a heuristic method based on the hybrid approach that uses search space reduction was developed and adapted to the optimal design of small off-grid PV irrigation systems with storage tanks.

On the other hand, as the pumping systems make the motor pumps operate at variable frequency, research work has also been dedicated to their modeling in this working condition: in [18], the application of pump similarity laws and the equations to calculate PV yields allowed a relationship between solar radiation and pump flow rate for a given pipeline; in [19], two mathematical models that linked the operating electrical power to the water flow rate of the pump versus total head were proposed; and in [20], two mathematical motor-pump models for PV applications were improved and validated.

There are also numerous simulation tools that make it possible to predict the productivity of PV pumping systems. The most relevant are mentioned here: DASTPVPS is a simulation tool developed by the Universität der Bundeswehr München [21]; PVSYSYS is the simulation tool probably most used in the professional world of photovoltaics (it is integrated with the solar radiation database METEONORM, and it also offers the possibility of simulating PV pumping systems); WinCAPS is the tool of the main Danish pump manufacturer [22]; COMPASS [23] is the tool of the main German pump manufacturer, and it is integrated with the solar radiation database provided by NASA; SOLARPAK is the tool of another world leader manufacturer of submersible motors [24]. All of them are just capable of simulating a single set of PV generator–frequency converter–motor pump, include default settings for inexperienced users, and use simple sizing methods such as the so-called “peak month” method. There are also other tools for the design and sizing

of irrigation networks, such as Hydrocalc [25] or GESTAR [26,27], and tools for irrigation requirements depending on the crop needs, such as CROPWAT [28].

These relatively small-power pumping systems with a single motor pump served mainly to supply drinking water to populations in developing countries where the conventional electrical networks necessary to raise water from the ground did not exist. However, the significant growth in electricity prices [29] has made electricity-intensive applications look for cheaper alternatives. This is the case of modernized irrigation in professional agriculture in first-world countries that has pumping stations fed by much larger powers (>1 MW) and with much more complex configurations, with several groups of motor pumps of different models and of different powers and connected to the conventional electricity grid.

In this context, large-power PV irrigation systems (PVISs) have been proposed and introduced to the market and are growing significantly. For example, Knech et al. wrote about a possible PV plant of 1800 kWp for a 12,000 ha farm in Patagonia [30]. Carrêlo et al. presented a comparative economic feasibility analysis of five large-power PVISs in the range from 40 to 360 kWp in the Mediterranean region [31]. Herraiz et al. technically studied the biggest one of the previous systems and a new one of 213 kWp in Spain [32]. Almeida et al. also technically studied one of the previous systems—a 140 kWp system in Portugal [33]. In addition, some other systems can also be found in Spanish news—a 121 kWp in Valladolid [34] or a 190.8 kWp in Albacete [35]. All these systems exceed the previous limit of 40 kW and reach the range of megawatts required by professional irrigators thanks to the fact that technical and economic barriers [36] have been removed—for example, the intermittent nature of the PV power was solved without the need of batteries, taking advantage of the energy regeneration of the motor pumps [37], and cost savings of up to 80% are shown in some real-scale experiences [31,34].

The appearance on the market of large-power PVISs to feed complex pumping stations has made it necessary to develop new simulation tools to simulate their performance. Some contributions to this need can already be found in the literature. It is worth mentioning the work of [38] in which a method for distributing the available PV power between two equal pumps working in parallel was proposed. The authors concluded that the power distribution ratio between the two pumps to maximize the water flow rate is 0% or 50% (i.e., just one operating pump or two with half available PV power each). There are also works that analyzed how to match the operation of the pumps to the demand in systems without limitation in the available energy that could be adapted for large-power PVISs [39,40].

However, it is not possible to find published works that allow the simulation of PVISs that feed more complex pumping stations such as those implemented in modernized irrigation. The difficulty in simulating the behavior of these systems when they are powered by a single PV generator lies in establishing the number of pumps that should be operating and their working frequency depending on the available PV power at every instant and, at the same time, establishing the hydraulic working point (water flow, Q , and pumping head, H) since the greater the number of pumps, the greater the water flow rate but also the pumping head, since friction losses in the pipeline increase due to the greater water flow. Dynamic input PV power and dynamic hydraulic duty point make it complex to solve the problem of calculating and simulating the maximum water flow rate pumped by the PVIS for a certain available PV power.

Objectives and Organization of the Article

The objective of this paper is to present new models that allow simulating the productivity of complex PVISs, such as those that exist in large-power pumping stations in irrigation communities. The models developed in this paper seek to maximize the water flow rate pumped at each moment according to the available PV power in large PVISs that work only with the PV generator (without the support of another power source and without the use of batteries). The models have been developed for pumping stations that

raise water to an elevated water pool but are easily transferable to direct pumping to the irrigation network (i.e., systems that work at constant pressure).

The models developed and presented here were implemented in the SISIFO tool (www.sisifo.info, accessed on 8 March 2022), the simulation tool of PV systems of the Universidad Politécnica de Madrid, and were used to analyze a real case study and illustrate the advantages of these models with respect to the current state of the art.

The paper is structured as follows: after this introduction, which justifies the novelty of this work, Section 2 presents the work development methodology, and Section 3 presents the new models developed. In Section 4, some interesting results are presented and discussed as a result of the application of these models to various configurations of PV irrigation systems and to a real case study. The paper ends with Section 5 presenting the main conclusions.

2. Materials and Methods

The methodology consists of two steps: the development of the models of two representative configurations of multipump PV irrigation systems and the application of the models to the simulation of a representative case study.

First, a system is modeled that consists of a group of several equal pumps in parallel that share a single PV generator and a hydraulic system, where at any given time, all or only part of the pumps may be active depending on the available PV power (Figure 2). Active pumps are synchronized in frequency, and the frequency value is calculated to maximize the water flow rate pumped. Frequency-synchronized equal pumps allow the modeling of an equivalent pump for each number of active pumps, which simplifies the calculation, as it is presented in Section 3.1. Therefore, the aim of this model is to select the combination of active–inactive pumps and working frequency that produces the highest water flow rate based on the available PV power at each moment.

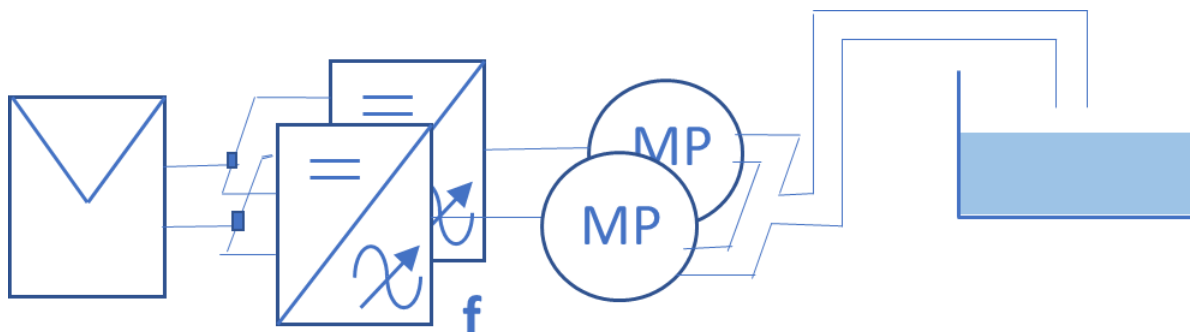


Figure 2. Model consisting of a group of several equal pumps in parallel that share a PV generator.

Second, a system consisting of two groups of pumps working in parallel and sharing the same PV generator and hydraulic system is modeled (Figure 3). This case allows using different pumps in each group. The model chooses the combination of active–inactive pumps and working frequency in each group that maximizes the total flow rate pumped based on the available PV power. Two variants are modeled:

1. The active pumps of the first group operate synchronized with each other at a fixed frequency (typically, it corresponds to the nominal frequency or the frequency at which maximum efficiency is achieved), and the active pumps of the second group operate synchronized with each other at a variable frequency;
2. The pumps in both groups operate at a variable frequency, and this frequency may be different in each group but equal within the same group.

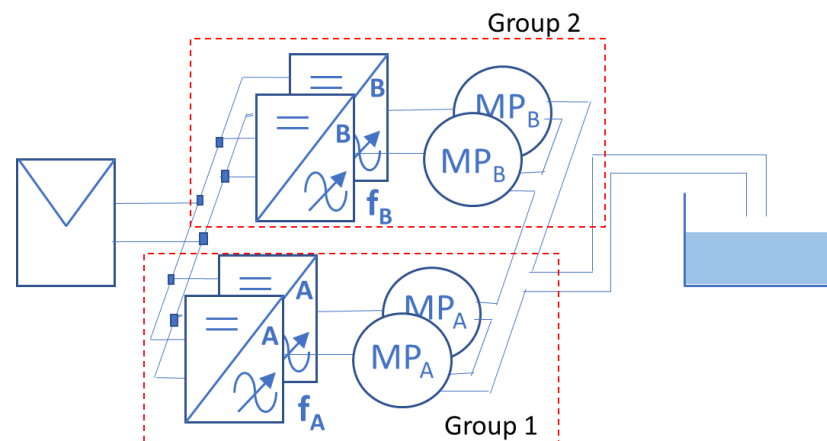


Figure 3. Model consisting of two groups of pumps working in parallel and sharing the same PV generator.

Finally, a case study is simulated to analyze, first, the details of the models and, second, the advantages of multipump models compared to the traditional methodology of simulation of these kinds of systems. The case study is based on a PV irrigation system of 3625 kWp located in Monegros (Spain) with a pumping station with a first group of five pumps of 500 kW each and a second group of two pumps of 200 kW each. The power rating of each frequency converter equals that of the pump to which it is connected.

3. Modeling of the Multipumping PV Irrigation Systems

3.1. Configuration 1: Multipump PVIS Made up of a Group of N Equal Motor Pumps, in Parallel and Synchronized in Frequency

The first step to model this configuration consists of obtaining the characteristic curves of an equivalent pump corresponding to N equal and frequency-synchronized pumps. The starting point is to obtain the characteristic curves of the individual pump at its nominal frequency, from the manufacturer's datasheet (Equations (1) and (2)):

$$H = k_{b0,1} + k_{b1,1}Q_1 + k_{b2,1}Q_1^2 \quad (1)$$

$$P_2 = k_{p0,1} + k_{p1,1}Q_1 + k_{p2,1}Q_1^2 \quad (2)$$

where H is the pumping head, P_2 is the demanded power at the pump input (or motor output), Q_1 is the water flow, and the parameters $k_{b0,1}$, $k_{b1,1}$, $k_{b2,1}$, $k_{p0,1}$, $k_{p1,1}$, and $k_{p2,1}$ are the parameters that fit the curves of the individual pump.

At a certain head H , the pump equivalent to N equal pumps working in parallel will pump a flow Q_N corresponding to the sum of the flow rates Q_1 that each individual pump elevates at the same head; therefore, from [1], it is simple to deduce that:

$$H = k_{b0,N} + k_{b1,N}Q_N + k_{b2,N}Q_N^2 = k_{b0,1} + k_{b1,1}Q_1 + k_{b2,1}Q_1^2 \quad (3)$$

where $Q_N = N * Q_1$, $k_{b0,N} = k_{b0,1}$, $k_{b1,N} = \frac{k_{b1,1}}{N}$, and $k_{b2,N} = \frac{k_{b2,1}}{N^2}$.

In the same way, from [2], it follows that the power $P_{2,N}$ necessary for the equivalent pump to pump a flow Q_N corresponds to the sum of the power P_2 of the N individual pumps when they pump a flow Q_1 :

$$P_{2,N} = k_{p0,N} + k_{p1,N}Q_N + k_{p2,N}Q_N^2 = N(k_{p0,1} + k_{p1,1}Q_1 + k_{p2,1}Q_1^2) \quad (4)$$

where $k_{p0,N} = N * k_{p0,1}$, $k_{p1,N} = k_{p1,1}$, $k_{p2,N} = \frac{k_{p2,1}}{N}$.

Figure 4 shows graphically the characteristic curves of the equivalent pump corresponding to N pumps, where $N = 1..5$.

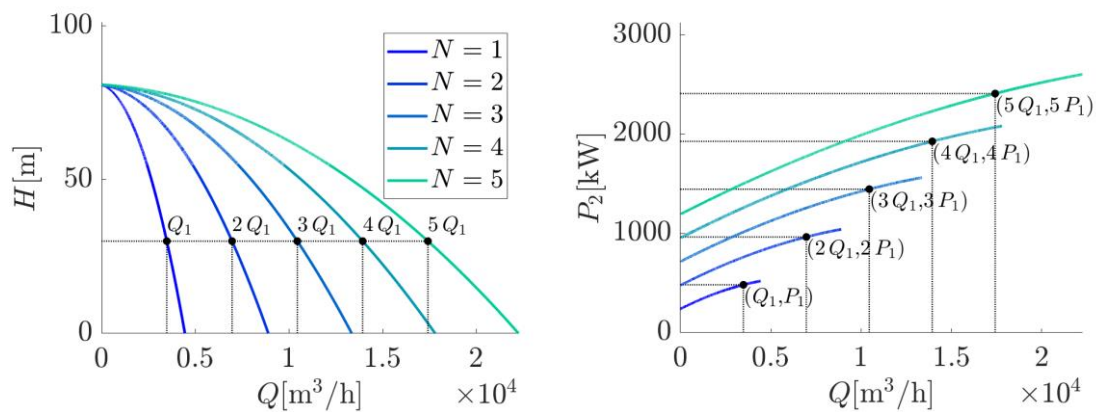


Figure 4. Characteristic curves of an equivalent pump corresponding to N equal and frequency-synchronized pumps, where $N = 1..5$.

On the other hand, the hydraulic system made up of a set of pipes of a certain diameter and length that connects the pumping station with the water pool imposes a Q - H curve that we call the “system curve” and that has the following expression:

$$H = k_{s0} + k_{s2}Q_1^2$$

where k_{s0} and k_{s2} are the parameters that fit the system curve.

As this equivalent pump operates at a variable frequency depending on the available PV power, $P_{DC,mpp}$, it is necessary to deduce the DC power, P_{DC} , needed to satisfy the one demanded by the pump, P_2 , at all possible Q - H working points within the range of frequencies at which it can operate. This calculation is made from the equivalent pump curves in three consecutive steps:

1. Determine the power P_2 demanded by the equivalent pump at a certain working point Q - H ;
2. Obtain P_{DC} at the input of the frequency converter corresponding to that P_2 , assuming that the motors of all pumps are identical;
3. Select the combination of active pumps that maximizes the flow rate pumped given the available PV power $P_{DC,mpp}$.

3.1.1. Calculation of P_2 for Any Q - H Working Point

To calculate the P_2 required by the equivalent pump working at a certain point (Q_B , H_B) not included in the Q - H curve at nominal frequency, the affinity laws are used following the procedure described in [41] but varying the head instead of the flow (Figure 5). Given a certain H_B :

1. Calculate the required flow Q_B as the real positive root for Equation (3): $0 = (k_{b0,N} - H_B) + k_{b1,N}Q_B + k_{b2,N}Q_B^2$ obtaining point B (Q_B , H_B) at frequency ω .
2. Determine the affinity parabola ($H = k_0 + k_2Q^2$) that passes through point B, where $k_0 = 0$, $k_2 = H_B/Q_B^2$. The affinity parabola connects the points of equal efficiency.
3. Calculate the intersection of the affinity parabola and Q - H characteristic curve of the pump at rated frequency, ω_{rated} , to obtain point C (Q_C , H_C).
4. Determine the hydraulic power at point C, $P_{HC} = \theta \cdot H_C \cdot Q_C$, where θ is a constant value that depends on the water density and gravity.
5. Determine P_2 at point C, $P_{2C}(Q_C)$ using Equation (4).
6. Calculate pump efficiency at point C, $\eta_{PC} = P_{HC}/P_2(Q_C)$, which is equal to the efficiency at point B, $\eta_{PB} = \eta_{PC}$.
7. Calculate the hydraulic power at point B, P_{HB} .
8. Finally, determine P_2 at point B as $P_{2B} = P_{HB}/\eta_{PB}$.

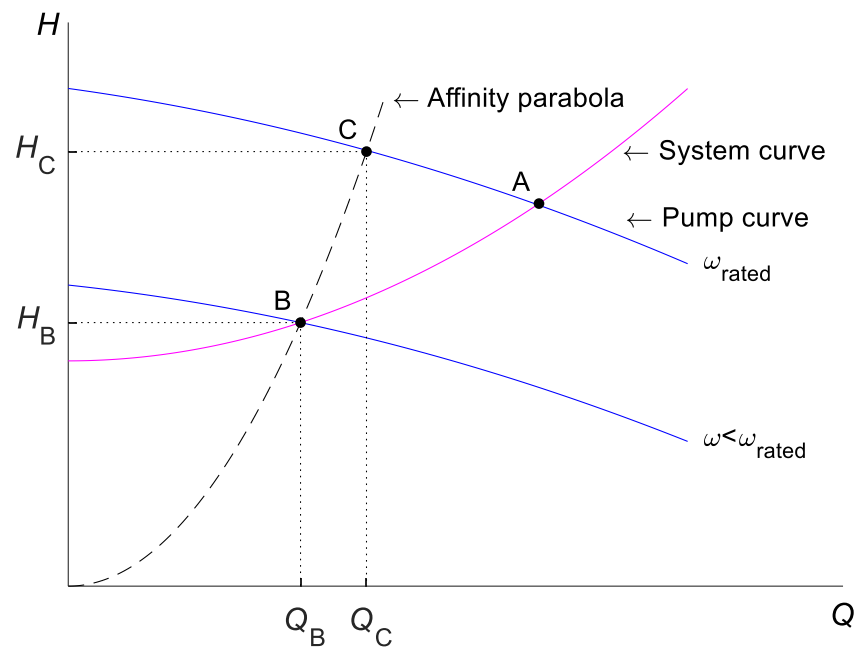


Figure 5. Illustration of the procedure to calculate the P_2 required by the equivalent pump working at a certain point (Q_B, H_B) . Point A would be the operating point on the system curve if the pump were operating at the rated frequency, ω_{rated} . Point B is the actual operating point at a lower frequency. The pump works at the same efficiency at point B as at point C, therefore allowing P_2 at point B to be calculated.

3.1.2. Calculation of P_{DC} at the Input of the Frequency Converter

The P_{DC} calculation depends on other elements present in the real system in which the pump operates, such as the pump motor, frequency converter, and the losses in the AC wiring between them. It is deduced from the value of P_{2B} according to the following algorithm:

1. Determine the power at the input of the motor (P_1) at point B: $P_{1B} = P_{2B} / \eta_M(P_{2B})$, $\eta_M(P_{2B})$ being the efficiency of the motor at P_{2B} .
2. Determine the power at the output of the frequency converter (P_{AC}), given the AC wiring losses W_{AC} at P_1 : $P_{AC,B} = P_{1B} / W_{AC}(P_{1B})$.
3. Determine P_{DC} : $P_{DC,B} = P_{AC,B} / \eta_{FC}(P_{AC,B})$, $\eta_{FC}(P_{AC,B})$ being the efficiency of the frequency converter at the load $P_{AC,B}$.

3.1.3. Selection of the Combination of Active Pumps That Maximizes the Pumped Water Flow

To obtain the highest water flow rate at the available DC PV power, $P_{DC, \text{mpp}}$, a procedure is necessary to select the number of operating pumps and the value of their synchronized frequency.

If we take S samples from the system curve, for each of the S values of H , we calculate Z values of Q , P_2 , and P_{DC} for each of the Z equivalent pumps resulting from the possible combinations of N pumps, where $Z = N$ as the N pumps are equal. Note that we will finally calculate S sets of Z values of Q , P_2 , and P_{DC} .

The P_{DC} - Q curve of each of the Z equivalent pumps may be fitted with a third-degree polynomial:

$$Q(P_{DC}) = k_{q0} + k_{q1}P_{DC} + k_{q2}P_{DC}^2 + k_{q3}P_{DC}^3 \quad (5)$$

Figure 6 shows an example of these fitted curves for the case of $Z = N = 5$ equivalent pumps. Given an available P_{DC} , it can be observed how it is possible to choose the highest flow rate as the maximum value of the different $Q = f_z(P_{DC})$, where $z = 1..Z$.

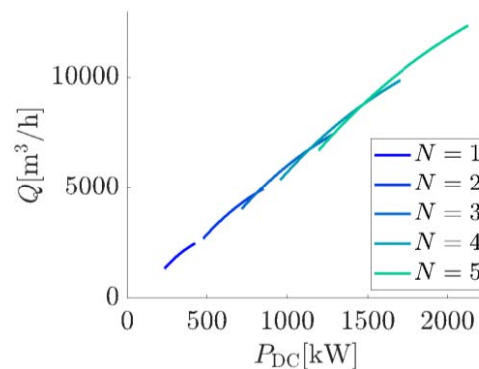


Figure 6. P_{DC} - Q curves of each of the equivalent pumps of a group of five equal and synchronized pumps.

Obviously, given a certain available $P_{DC, mpp}$, not all the Z equivalent pumps are eligible because each one of them works in a certain P_{DC} range; therefore, the selection procedure applies a series of restrictions:

- The minimum DC power of the equivalent pump (P_{DCmin}) that is determined by the minimum cooling water flow of the pumps (Q_{min}) that its manufacturer requires. This restriction disables some combinations of pumps. It should be noted that Q_{min} of the equivalent pump is different from N times the minimum one of the individual pump due to the higher working head in the system curve.
- The maximum DC power of the equivalent pump (P_{DCmax}), which is determined by the maximum operating frequency of each individual pump (ω_{max}). The equivalent pump is still eligible but is limited to this maximum operating frequency even if more power is available ($P_{DC, mpp} > P_{DCmax}$). Again, note that the power demanded at this ω_{max} by the equivalent pump is different from N times that of an individual pump, also due to the higher working head in the system curve.

It is worth mentioning that we are considering frequency-synchronized pumps; therefore, when they use the same model of motor and frequency converter and there are the same wiring losses, each of the frequency-converter-wiring-motor-pump sets active at every moment demands the same DC power.

3.2. Configuration 2: Group of N Equal Pumps + Group of M Equal Pumps

In real PVISs, it is common to find pumping stations with two different groups of pumps. Typically, there is a group of N equal, high-power pumps driven by soft starters and therefore operating at their fixed nominal frequency. The other group consists of M equal pumps but of lower power than those of the previous group, and, in addition, they are driven by frequency converters, which allows them to work at a synchronized but variable frequency. It can also be found that the first group also has frequency converters and that, therefore, they can also work at a synchronized and variable frequency. Pump groups are modeled following the process described in configuration 1.

The number of active pumps in each group is selected again to maximize the pumped flow rate depending on the available PV power.

3.2.1. Selection of the Combination of Pumps

Dynamic programming (DP) was chosen as the selection methodology due to its suitable characteristics because this case (a) presents an optimal substructure, as an optimal solution for n active pumps meeting a water flow and head requirement contains a suboptimal solution for $n - 1$ active pumps, and (b) presents overlapping subproblems because the power that a single pump demands when it is pumping a water flow at a given head may be part of several suitable solutions.

DP is applied in a bottom-up approach, where all possible small problems are solved and then combined to obtain solutions for bigger problems. DP is an optimization method based upon the use of Bellman's optimality principle [42], which establishes that "An

optimal policy has the property that whatever the initial state and initial decision are, the remaining decisions must constitute an optimal policy with regard to the state resulting from the first decision". As stated in [40] where DP is applied to optimize grid-connected pumps, this can also be expressed as: "given an optimal trajectory from point A to point C, the portion of the trajectory from any intermediate point B to point C must be the optimal trajectory from B to C" [43].

Applying it to our case, this principle results in solving the recursive Equation (6):

$$f_z(x) = \min_{0 < x_z < x} [g_z(x_z) + f_{z-1}(x - x_z)] \quad (6)$$

with $z = 1, 2, \dots$ $f_1(x) = g_1(x)$ $x > 0$.

Where z corresponds to each combination of active pumps, with $1 < z < Z$; x corresponds to the constrained state variable, which is the required water flow, Q_s , at the system curve discretized in S samples (where $1 < s < S$), and therefore it implies a working head, H_s , that all z active pumps must meet; $g_z(x)$ is the state cost function, for this case, the demanded DC power by a single pump while pumping a water flow Q_z at H_s , $P_{DC,z}$; $f_{z-1}(x)$ is the cost of the rest of the path, hence the demanded DC power of the rest of $z-1$ active pumps, $P_{DC,z-1}$, pumping the rest of water flow, $Q_s - Q_z$ at H_s . Therefore,

$$P_{DC,z}(Q_s) = \min_{0 < Q_z < Q_s} [P_{DC,z}(Q_z) + P_{DC,z-1}(Q_s - Q_z)] \quad (7)$$

In this work, the aim is to maximize the volume of water pumped; therefore, for each instance, the highest flow rate Q_s where the required power $P_{DC,z}(Q_s)$ does not exceed the available power from the PV generator, $P_{DC,mpp}$, is chosen. Therefore,

$$Q_{s,max} = \max_{0 < Q_s < Q_s} [Q_s | P_{DC,z}(Q_s) \leq P_{DC,mpp}] \quad (8)$$

Each subset of active equal frequency-synchronized pumps can be reduced to an equivalent pump, as exposed above, simplifying the required calculation.

3.2.2. Subconfiguration 2.1: A First Group of N Pumps at Fixed Frequency and a Second Group of M Pumps at Variable Frequency

In this subconfiguration, the pumps in the first group work synchronized at a fixed nominal frequency, and the second group of pumps works synchronized at a variable frequency.

If the first group consists of N pumps and the second of M pumps, there are $Z = (N + 1) \times (M + 1) - 1$ combinations depending on the number of active pumps. The equivalent pumps for the combination of n active pumps of the first group, where $n = 0..N$, and for the combination of m active pumps of the second group, where $m = 0..M$, can be modeled using Equations (3) and (4). However, unlike in configuration 1, the points (H_n, Q_n) and (H_m, Q_m) where each group of pumps operates are not on the system curve.

If the system curve is discretized in S points (Q_s, H_s) where $1 < s < S$, for each H_s , the second group of pumps must pump the difference between the flow of the first group, Q_n , and the total flow Q_s at the height H_s (see Figure 7). The first group operates at the point (Q_n, H_s) of the equivalent $Q-H$ nominal curve of n active pumps. The second group operates at the point $(Q_s - Q_n, H_s)$ on the equivalent $Q-H$ curve of m active pumps at the frequency necessary to contain said point.

It is obvious that, in the case $n = 0$, or $m = 0$, the system is reduced to configuration 1, since only the pumps of the first group, or of the second group, are active, respectively.

As an example, Figure 7 shows the case $N = 2$ and $M = 1$ and the working point when $n = 2$ and $m = 1$ pumps are active at H_s .

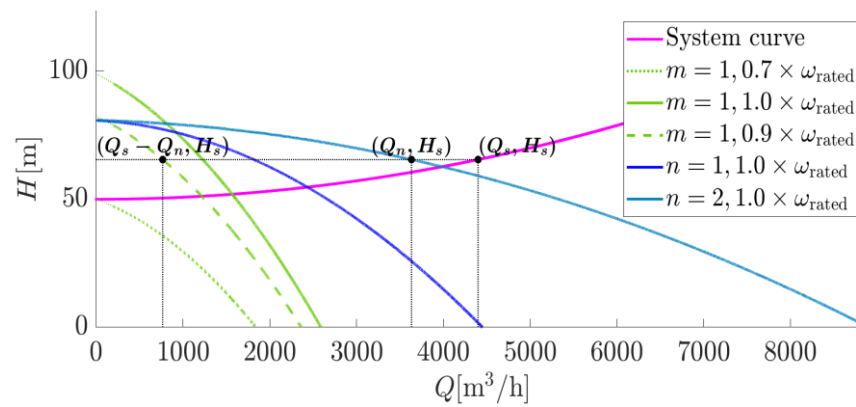


Figure 7. For the case $N = 2$ and $M = 1$, Q - H curves and the working point when $n = 2$ and $m = 1$ active pumps at H_s .

Using the described procedure of selection of the combination of pumps, the active pump combination (n, m) that pumps the highest flow rate at the available PV power is obtained, and the combinations that demand more DC power or that would force the pumps to operate at frequencies outside of its range are discarded.

Figure 8 shows in red the Q - H locus where the second group of variable frequency pumps is required to work for each combination of n active pumps in the first group. Shaded in gray, the locus for which there is no solution, i.e., for each head, the flow rate pumped by each pump group separately, or the combination of both, does not reach the required flow rate in the system curve. Obviously, when $n = 0$, this locus is the system curve itself.

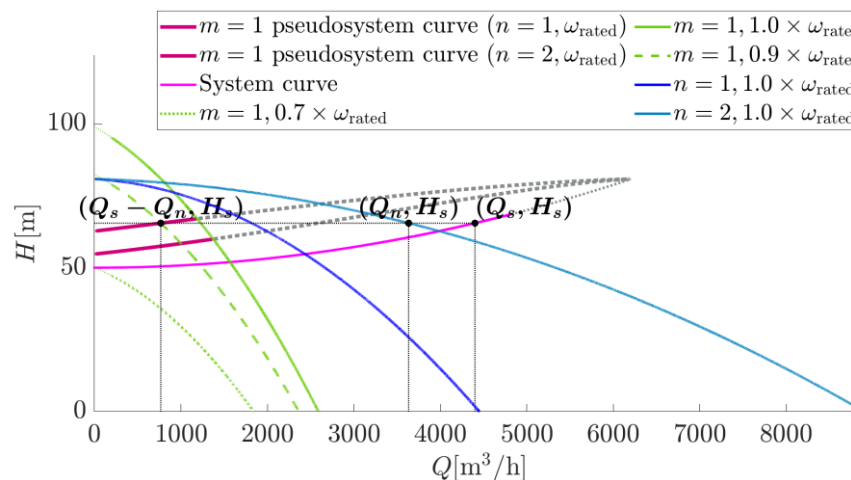


Figure 8. Q - H curves and working points for the case $N = 2$ and $M = 1$ and the Q - H locus where the second group of variable frequency pumps is required to work for each combination of n active pumps in the first group.

This set of z_n locus (H, Q) of the second group of pumps can be modeled with third-degree polynomials that would constitute z_n “pseudo system curves” for the second group of pumps (Equation (9)).

$$H(Q) = k_{z_n0} + k_{z_n1}Q + k_{z_n2}Q^2 + k_{z_n3}Q^3 \tag{9}$$

The point of this pseudo curve at H_s determines the frequency of the second group of m active pumps.

Figure 9 shows the P_{DC} - Q curves for each combination of (n, m) active pumps for the case $N = 2$ and $M = 2$, where Q is normalized to its maximum value. For each combination,

the flat part of the curve corresponds to all active pumps operating at their maximum (nominal) frequency.

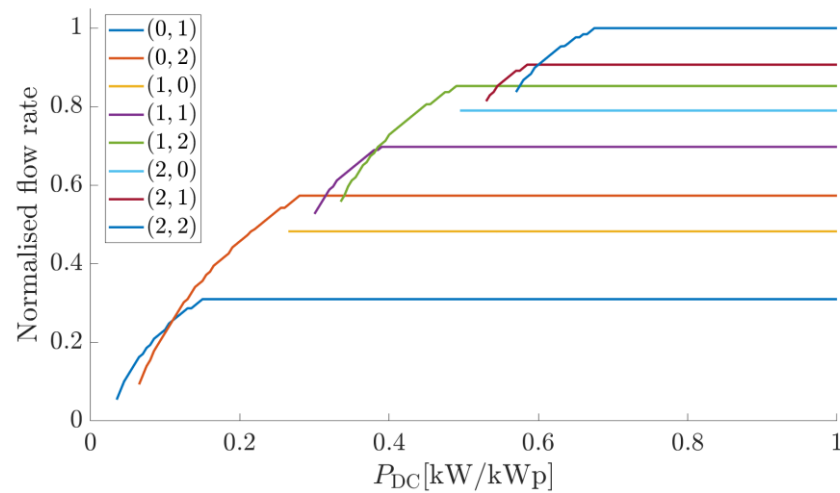


Figure 9. P_{DC} - Q curves for each combination (m, n) of active pumps for the case $N = 2$ and $M = 2$.

Figure 10 allows analyzing the operation of the system showing, depending on the available P_{DC} , (a) the rate flow normalized to its maximum value (blue line in both Figure 10a,b), which is the envelope curve of Figure 9; (b) the chosen combination of (n, m) active pumps (dashed blue line in both Figure 10a,b); (c) the working frequency of the n -pump group normalized to its maximum value (orange line in Figure 10a); (d) the working frequency of the m -pump group normalized to its maximum value (yellow line in Figure 10a); (e) the ratio of P_{DC} demanded by the n -pump group, normalized to P_{DC} value (orange line in Figure 10b), i.e., 1 when the n -pump group is the only one operating and consuming all the power, 0.5 when both groups of pumps demand an equal power, and 0 when the n -pump group is stopped; (f) the power not used by the system, $P_{DC, mpp} - P_{DC}$ (yellow line in Figure 10b); and the efficiency of each group of pumps (dotted purple and green lines in Figure 10b) in terms of hydraulic power (P_H) regarding the DC power consumed by the group of pumps ($P_{DC, n}$ or m -pumps).

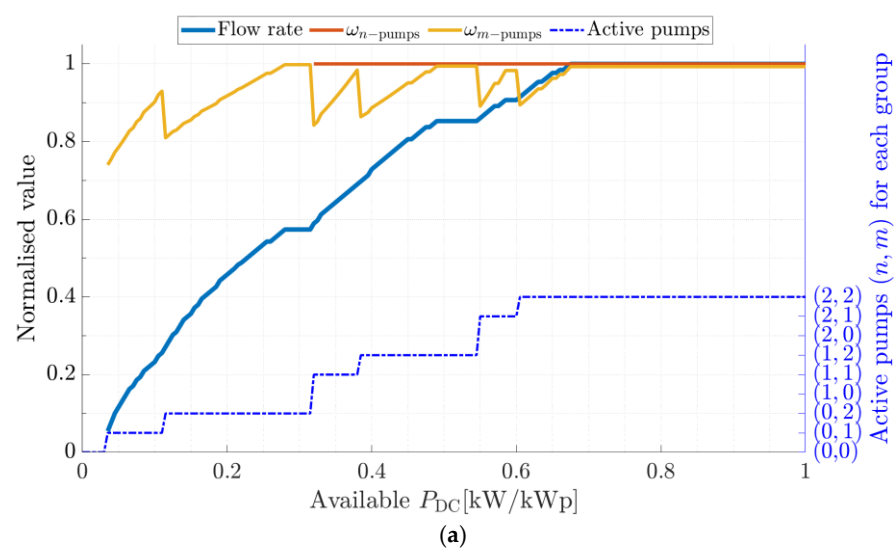


Figure 10. Cont.

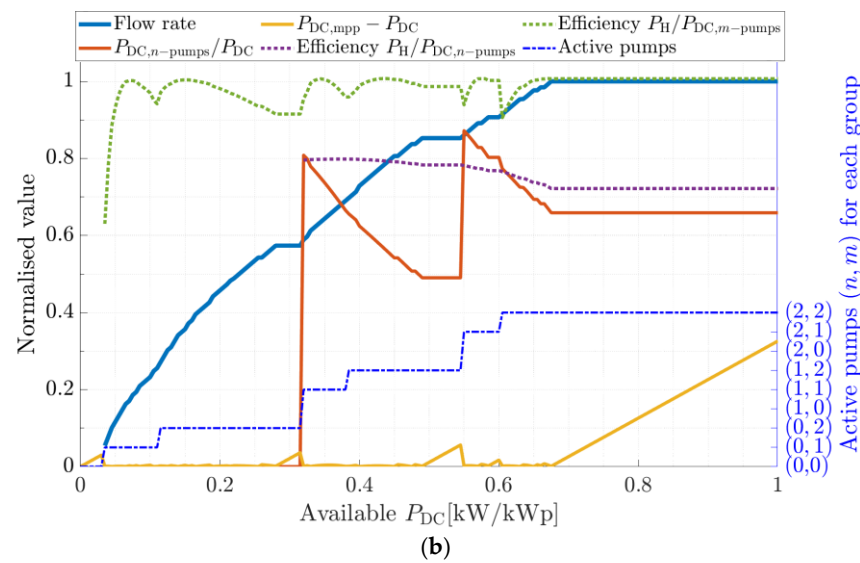


Figure 10. For the case $N = 2$ and $M = 2$, combination of pumps that maximizes the water flow pumped depending on available P_{DC} , as well as the frequency at which the two groups of pumps will work; (a) operation view—working frequencies, (b) design view—efficiencies, power balance, not used P_{DC} .

3.2.3. Subconfiguration 2.2: Two (or More) Groups of Pumps Working at Variable Frequency

This configuration consists of a first group of N pumps working at a variable synchronized frequency and a second group of M pumps also working at a variable synchronized frequency that does not have to be the same as the one of the first group. Here, the case of two groups of pumps is modeled, but the model is valid for a greater number of groups.

In the same way as subconfiguration 2.1, each group of pumps is modeled with its equivalent pump and the number of active pumps in each group, n and m , and their frequencies are calculated by the same selection algorithm described there to maximize the water flow pumped at the available P_{DC} .

The only difference is that the selection algorithm is more complex, since the set of “pseudo system curves” for the different equivalent pumps of the second group of pumps is actually a “pseudo system area” because there is no single water flow rate for each equivalent pump of the first group of pumps, Q_n , at the head H_s , but there is a range of Q_n values since it can work at different frequencies and not only at the nominal frequency.

Figure 11 shows, for $N = 2$ and $M = 1$, the “pseudo system area” (pink area) when $n = 2$ and $m = 1$.

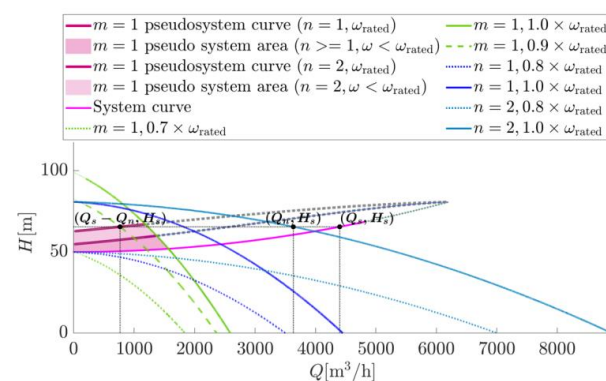


Figure 11. Q - H curves and working points for the case $N = 2$ and $M = 1$, and the Q - H “pseudo system area” where the second group of variable frequency pumps is required to work for each combination of n active pumps working at variable synchronized frequency in the first group.

Figure 12 shows, for $N = 2$ and $M = 2$, the combination of pumps and their frequency that would maximize the water flow pumped depending on the available P_{DC} , together with the rest of the variables shown in Figure 10.

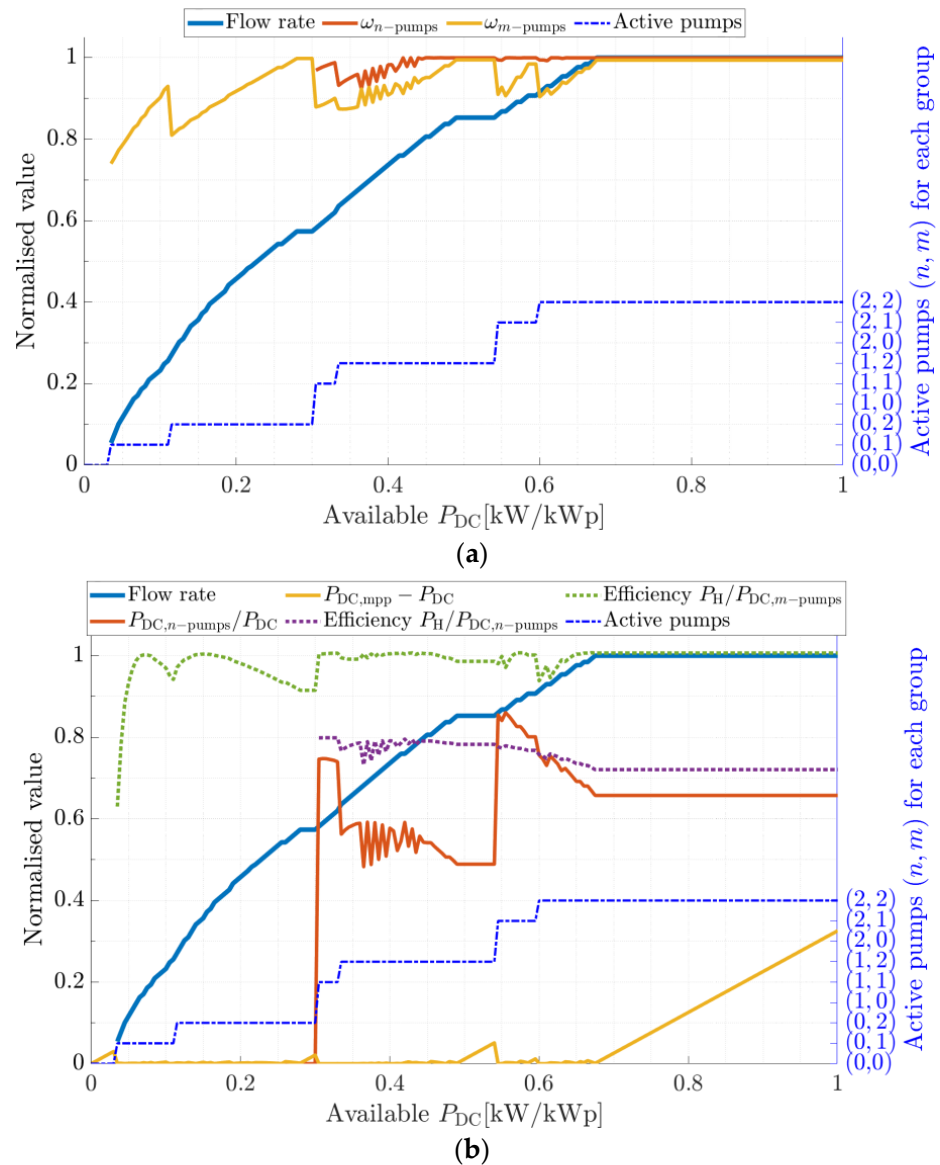


Figure 12. For the case $N = 2$ and $M = 2$, combination of pumps that maximizes the water flow pumped for a certain available P_{DC} , as well as the frequency of the two groups of pumps; (a) operation view—working frequencies, (b) design view—efficiencies, power balance, non-useful P_{DC} .

4. Results and Discussion

The described models were applied to a system to be installed in Monegros (Spain), lat = $41^{\circ}30'03''$ N, lon = $0^{\circ}02'125''$ W, using the Typical Meteorological Year offered by PVGIS as meteorological data. This system consists of a first group of five equal frequency-converter-motor-pump sets, each with a rated power of 500 kW, and a second group consisting of two frequency-converter-motor-pump sets with a lower power of 200 kW. Both groups share a 3625 kWp PV generator mounted on a North-South horizontal axis tracker. Figure 13 shows the characteristic curves for each $(n, 0)$ and $(0, m)$ combinations of active pumps, as well as the system curve.

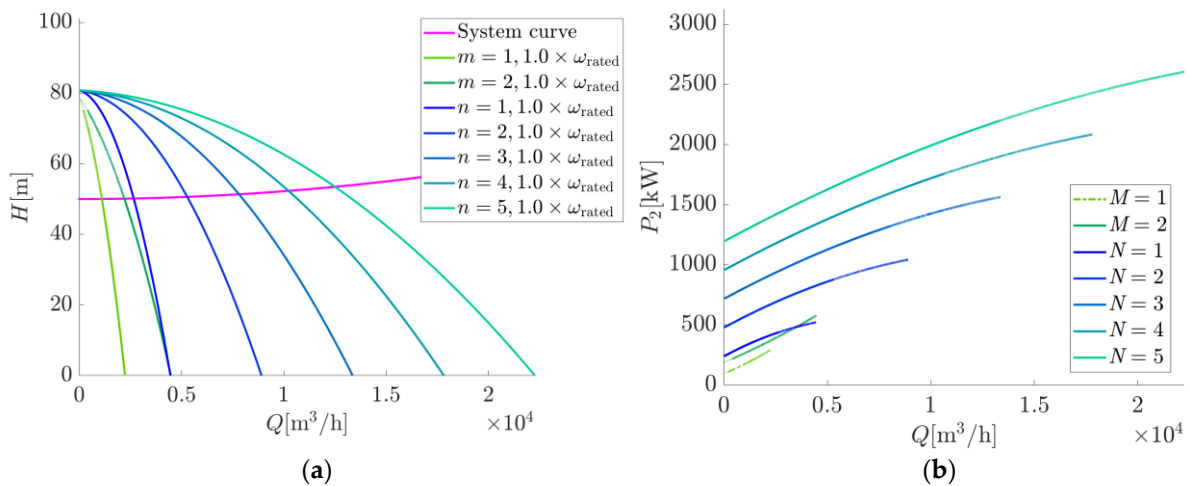


Figure 13. H - Q and P_{DC} - Q characteristic curves—(a) and (b), respectively—for each of the equivalent pumps for $N = 5$ and $M = 2$.

Three different analyses are performed, and their results are discussed.

In Section 4.1, the difference in pumped volume is compared when considering several frequency-converter-motor-pump sets connected to independent PV generators, with respect to the same number of sets sharing the complete PV generator.

Section 4.2 analyzes the difference in the water volume pumped based on the type of frequency control used, specifically, frequency-synchronized groups of motor pumps with respect to the ones operating at different frequencies, either both variable or one of them at their fixed nominal frequency and the other one variable.

Finally, Section 4.3 describes the pumped volume expected for the complete system ($N = 5$, $M = 2$) using subconfigurations 2.1 and 2.2 in order to observe the difference in production when the first group operates at nominal frequency vs. when operating at variable frequency, in both cases complemented by a group of $M = 2$ small pumps synchronized at variable frequency.

4.1. Independent PV Generators vs. Shared PV Generator

Existing simulation tools were just able to simulate a single frequency-converter-motor-pump set by adapting its frequency to the available power from a PV generator with rated power $P_{\text{nom}1}$ (hereafter referred to as the base case, Figure 14a). Therefore, to simulate a group of N pumps synchronized at a variable frequency and sharing a PV generator of rated power $N \times P_{\text{nom}1}$ (hereafter referred to as the N -case, Figure 14b), the volume pumped simulated in the base case was multiplied by N . It was known that this assumption is somewhat erroneous because, in conditions of low irradiance (early and late morning or cloudy days), the volume pumped in the N case should improve the volume pumped in the base case. It was because, at certain times, the base case PV generator may not generate enough power to activate the pump but N times this power (N case) could be enough to activate a subset of the n pumps, $0 < n < N$, even if it was not enough to activate all N pumps.

Using the model described in configuration 1, it is possible to observe this gain. For this purpose, the first set of large pumps ($N = 5$) was simulated and compared to the base case ($N = 1$). Figure 15 shows the evolution of the yearly gain, varying $N = 1..5$, in relative terms, when the hydraulic piping system is also resized (solid line), to obtain similar friction losses for each N . It can be observed that this gain reaches the value of 8.5%. The “piping system resized” gain is representative of an irrigation system with well-designed pipes with an appropriate diameter.

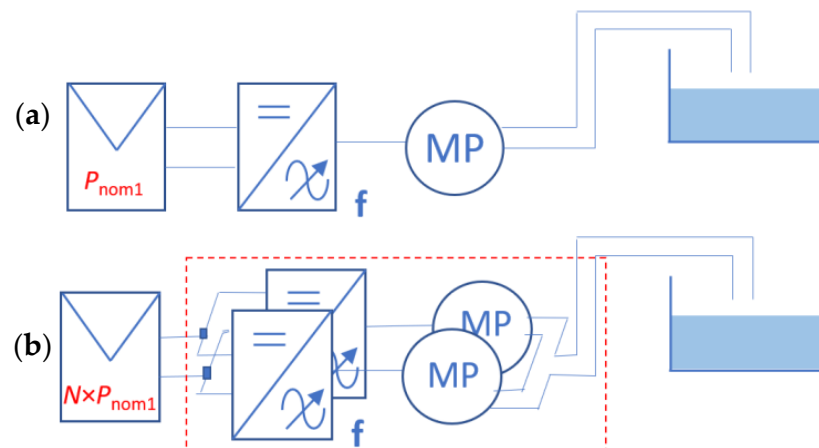


Figure 14. (a) A single pump connected to a single PV generator of P_{nom1} . (b) Group of N pumps sharing a single PV generator of $N \times P_{nom1}$.

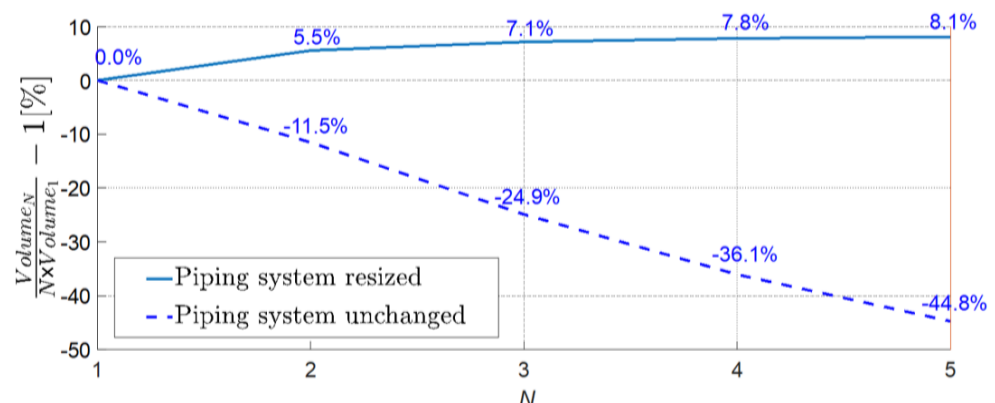


Figure 15. Relative gain of the volume pumped in the N case with respect to the base case with and without resizing the hydraulic piping system.

The “piping system unchanged” gain (dotted line in Figure 15) is representative of systems without the possibility of widening the diameter of the water distribution pipes and therefore increasing the friction losses when increasing N . In this case, in the multipump simulation (N case), not only no gains are obtained but also losses of 44.8% with respect to the traditional simulation method (base case and multiplying by N).

4.2. Performance vs. Type of Frequency Control

Here, the models developed are used to compare the difference in the volume of water pumped as a function of the type of frequency control implemented. For simplicity and to better observe the results, only two of the higher power pumps (500 kW) are considered ($N = 2$). Three frequency controls are applied: (a) both pumps work synchronized at a variable frequency; (b) one pump works at a constant (nominal) frequency, and the second pump works at a variable frequency; and (c) one pump works at a variable frequency, and the second pump also works at a variable frequency, which can be different. Control (a) is modeled by defining a single group of two pumps synchronized in frequency and applying configuration 1. Controls (b) and (c) are modeled using configurations 2.1 and 2.2, respectively, with the singularity that both groups of pumps contain the same model of pump. This allows simulating different frequencies in each group. Figure 16 illustrates the three controls, respectively. In all the cases, the PV generator and the hydraulic system are shared.

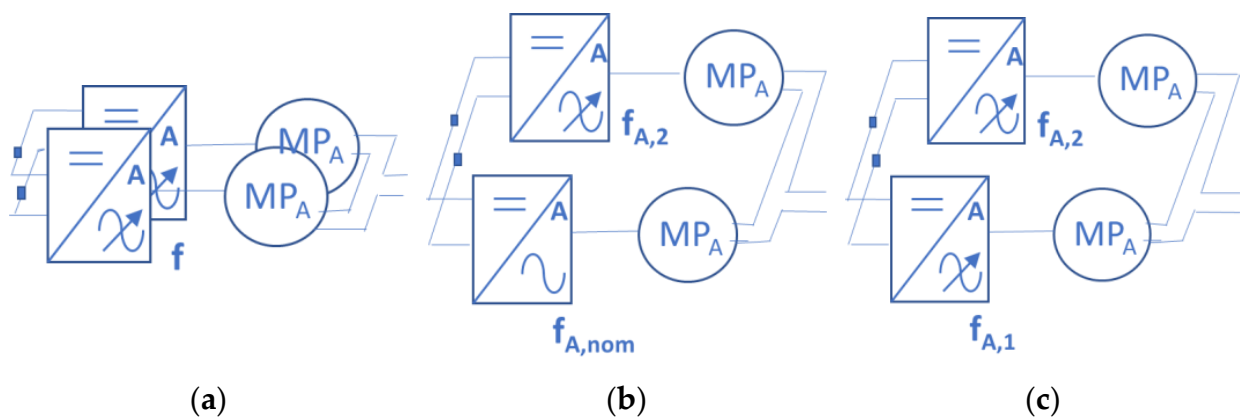


Figure 16. Three possible frequency controls under comparison: (a) both pumps work synchronized at a variable frequency, (b) one pump works at a constant (nominal) frequency, and the second pump works at a variable frequency, and (c) one pump works at a variable frequency, and the second pump also works at a variable frequency, which can be different.

Table 1 shows some relevant yearly results: potential DC energy yield of the PV generator working at maximum power point (MPP) without the limitations imposed by the motor pump, actual DC energy yield because of the pump limitation, AC energy yields at the input of motor, hydraulic energy yield and water volume obtained over a typical meteorological year.

Table 1. Simulated yearly relevant results for each type of control.

| | Frequency Control Type | | |
|--|-----------------------------------|--|---|
| | Control (a) $N = 2$ (Variable) | Control (b) $N = 1$ (Nominal) $M = 1$ (Variable) | Control (c) $N = 1$ (Variable) $M = 1$ (Variable) |
| Potential DC energy yield at MPP, $E_{DC,MPP}$ (kWh/kWp) | 2057.9 | 2057.9 | 2057.9 |
| DC energy yield, E_{DC} (kWh/kWp) | 1936.3 | 1924.0 | 2036.9 |
| $E_{DC}/E_{DC,MPP}$ ratio | 0.950 | 0.935 | 0.990 |
| AC energy yield at the motor-pump input, E_1 (kWh/kWp) | 1859.7 | 1747.7 | 1860.5 |
| Mechanical energy yield at the pump input, E_2 (kWh/kWp) | 1690.0 | 1567.1 | 1690.7 |
| Hydraulic energy yield, E_H (kWh/kWp) | 1439.5 | 1326.2 | 1440.1 |
| Annual water volume yield (m^3/kWp) | 9868 | 9141 | 9872 |

As expected, controls (a) and (c) where both pumps are running at variable frequency show a higher annual volume than control (b) (>8%), and control (c) slightly exceeds control (a). The differences come when there is enough power available to activate more than one pump but not yet enough for all pumps to be active and at their nominal frequency and have two complementary causes:

- In control (b), there is a larger range of $P_{DC,mpp}$ values that cannot be fully exploited, mainly because there is not enough power available yet to start the large pump at its nominal frequency while the small pump is already operating at its nominal frequency.
- The efficiency of the converter, wiring, motor, and pump assembly is different for each duty point. In case (c), there are duty points corresponding to two pumps working at different frequencies that provide more total water flow than the other duty points with frequency restrictions (either one pump is forced to nominal frequency or both pumps are forced to equal frequencies). In other words, the higher efficiency of one pump can compensate for the worse efficiency of the other pump and overcome the combination where both pumps must operate at the same efficiency. The final gain is small compared to control (a) but appreciable. This gain improves if the number of

pumps is increased. In the literature, some studies can be found in which this gain is neglected and the $P_{DC,mpp}$ is assumed to be equally distributed between both pumps, perhaps due to the impossibility of predicting a different distribution, as this requires a solution such as the one proposed in this work, using dynamic programming.

Obviously, it depends on the parameters of the system elements. Furthermore, when applied to different sites, the different frequency distribution of the power available at the site can amplify or minimize each effect.

4.3. Performance of a Study Case $N = 5$ and $M = 2$

Here, the real system in Los Monegros is simulated. Two cases are considered: (a) $N = 5$ (at nominal frequency), $M = 2$ (at a variable frequency) and (b) $N = 5$ (at a variable frequency), $M = 2$ (at another variable frequency). The nominal power of the shared PV generator is 3625 kW (AC/DC ratio = 0.8).

Table 2 shows the yearly results of both configurations. The difference in annual pumped water flow is 2.1% in favor of control (b). Control (a) allows the large pumps to operate at nominal frequency, with the second group of pumps operating at variable frequency to adapt the water flow to the available P_{DC} at any given time. This control (a), therefore, protects more the reliability of the large pumps, which operate at nominal power without a significant loss of productivity, and simplifies the control of both groups of pumps.

Table 2. Simulated yearly results for the two configurations in Los Monegros.

| | Control (a) | Control (b) |
|--|-------------|-------------|
| Potential DC energy yield (at MPP), $E_{DC,MPP}$ (kWh/kWp) | 2057.9 | 2057.9 |
| DC energy yield (MPP), E_{DC} (kWh/kWp) | 1990.3 | 2000.1 |
| $E_{DC,MPP}/E_{DC}$ ratio | 0.967 | 0.972 |
| AC energy yield at the motor-pump input, E_1 (kWh/kWp) | 1922.5 | 1936.2 |
| Hydraulic energy yield, E_H (kWh/kWp) | 1553.1 | 1586.3 |
| Annual water volume yield (m^3/kWp) | 10,741 | 10,962 |

Figure 17 is very useful to analyze the performance of the system in the two cases. In the design view (Figure 17b,d), dotted blue lines show the active pumps depending on the available PV power while red lines show the ratio of the total power consumed by the active pumps of the group N , and some relevant conclusions can be drawn from their analysis. For example, the lower number of steps in the dotted blue line of control (b) indicates a lower number of start–stop events of the pumps with the variation of the available PV power, which is beneficial from the point of view of long-term reliability of motor pumps.

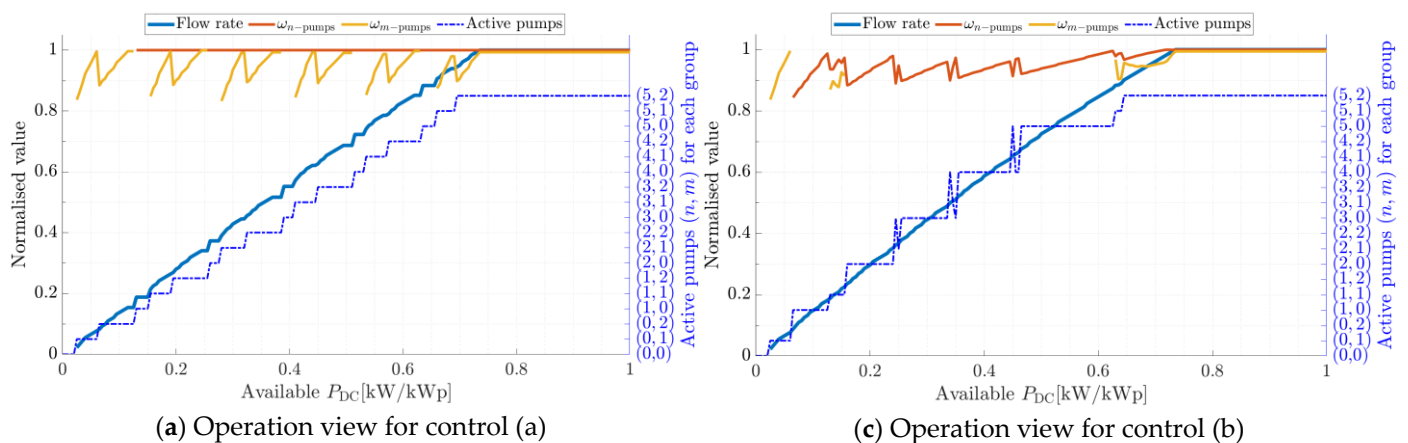


Figure 17. Cont.

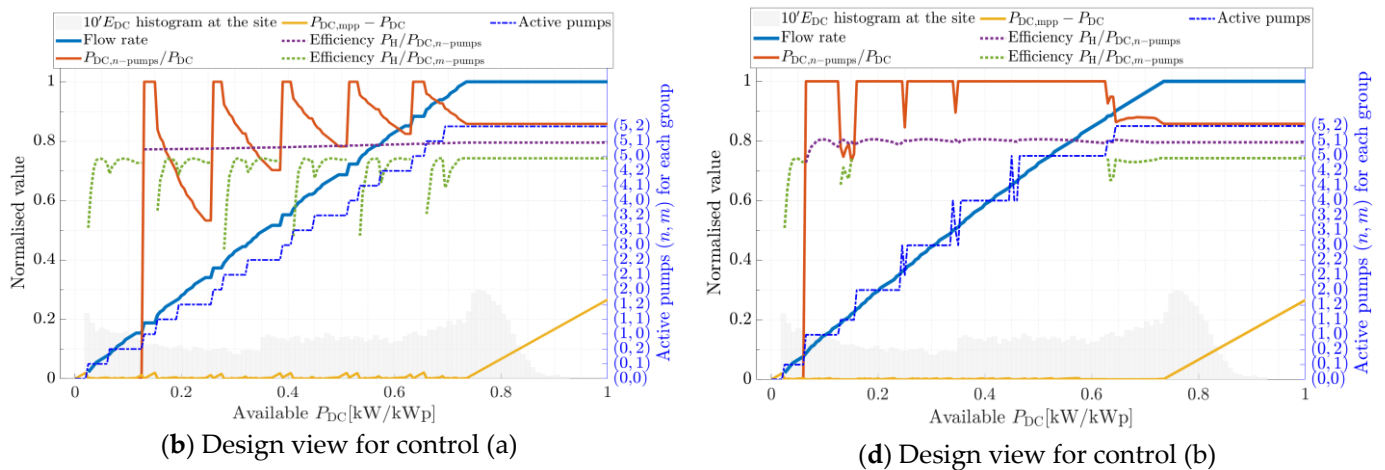


Figure 17. Combination of pumps that maximizes the water flow pumped for a certain available P_{DC} , as well as the frequency at which the two groups of pumps will work in control (a)— n pumps at nominal frequency and m pumps at variable frequency; and in control (b)— n pumps at a variable frequency and m pumps at other variable frequency.

The analysis of the orange lines in design views shows how in control (b), and for values of normalized available PV power less than 0.6, the larger pumps (the ones of group N) absorb the whole available power, except for very low available PV power. This means that large-power pumps are more efficient, and their use is preferable to small-power pumps. However, in case control (a), an increased use of small pumps is required as the large ones must work just at nominal frequency. This is the reason why case control (b) shows better yearly results in Table 2. However, this increase in performance comes at the price of having five more frequency converters.

Operation view (Figure 17a,c) is not only useful for simulation purposes but also to implement the control algorithms when installing the real PVIS.

Figure 18 allows an analysis on a daily basis. A clear day and a cloudy day were selected, and both of the above controls were applied. From the point of view of the greater volume of water pumped in this work, it can be seen that the origin of the difference in favor of control (b) shown in Table 2 comes mainly from the greater production of the system on cloudy days or in conditions of average irradiance. For example, on the cloudy day 169 of 365, control (b) (Figure 18b) manages to pump $29.9 \text{ m}^3/\text{kWp}$ compared to 28.1 m^3 for control (a) (Figure 18a), i.e., 6.4% more. Part of this difference is due to the higher efficiency of the pump at working points in control (b) (dotted blue and red lines in Figure 18), but another part is due to the fact that 1.67% of the available daily energy could not be used because there was no possible working point for the system in control (a) (yellow line at design view in Figure 17), compared to 1.0% of the daily energy not used in control (b), mainly at the beginning and end of the day. In contrast, in high-irradiance conditions, such as day 188 of 365, control (b) (Figure 18d) manages to pump $45.9 \text{ m}^3/\text{kWp}$ vs. $45.1 \text{ m}^3/\text{kWp}$ of control (a), only 1.7% more. This better result in pumps synchronized in frequency with respect to some pumps working at nominal frequency coincides with what has been stated by other authors for the case of grid-connected systems [44].

The use of this tool to better adapt the design of the system to the climatology of the PV generator location and the greater complementarity between large and small pumps in pursuit of one or more objectives, such as minimizing the number of starts/stops, reducing the number of frequency converters needed, better withstanding fades in irradiance due to passing clouds, taking advantage of all the energy that the PV generator can produce at its maximum power point, or forcing higher-efficiency duty points for some pumps are some of the main advantages of the models developed in this paper.

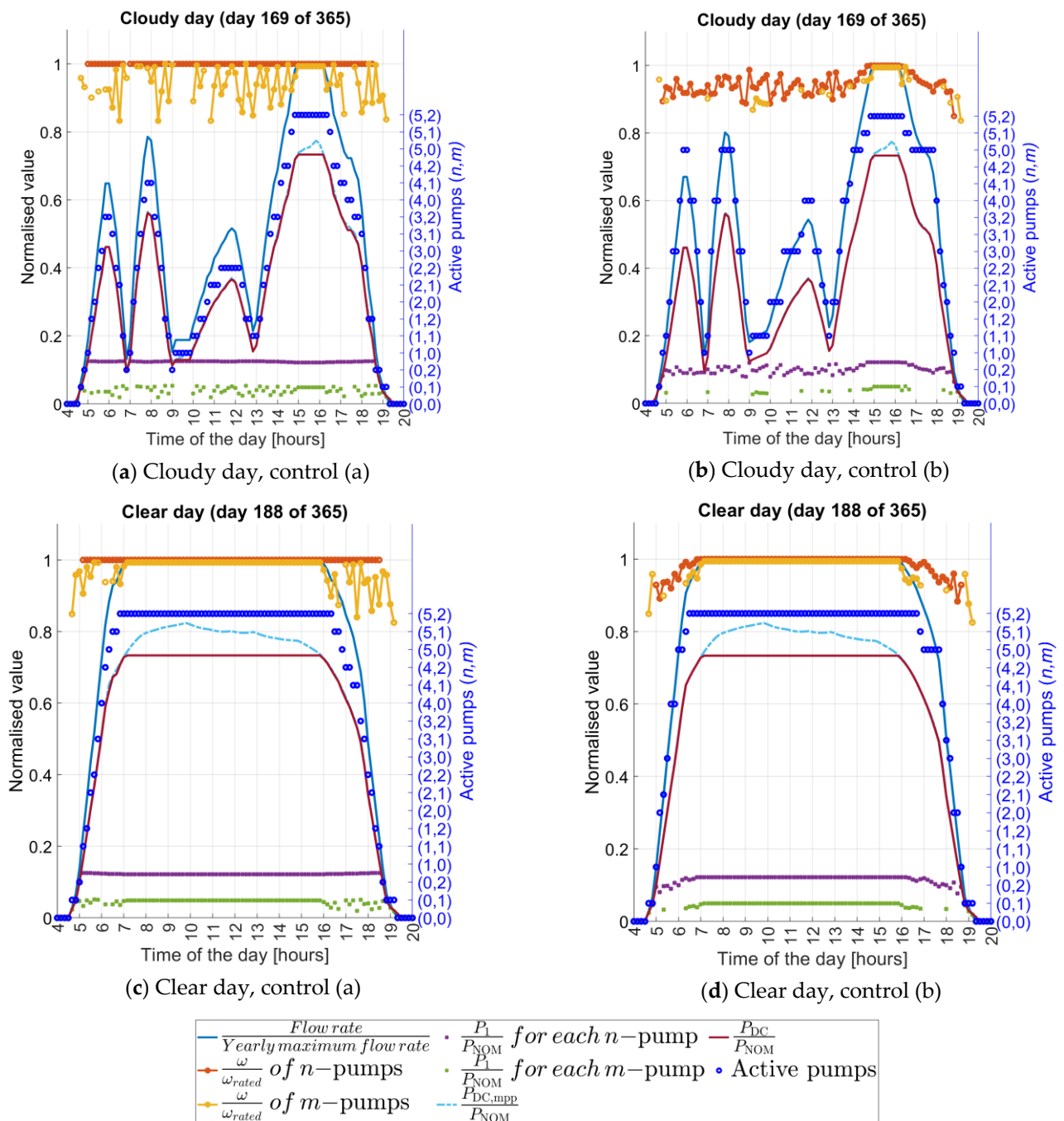


Figure 18. Cloudy and clear day. Case $N = 5$ and $M = 2$. (As there are two groups of different pump types, the best combination (with the chosen criteria) can include 0 or more active pumps in each group. A line disappears (discontinuous effect) in those combinations where there are 0 active pumps in one of the groups).

5. Conclusions

The growing market of large-power PVISs to power pumping stations, with several pumps, even of different models and nominal powers, working in parallel, requires simulation tools with the capability of estimating the productivity of these multipump systems. This was precisely the objective of this paper: to develop simulation models of multipump PV irrigation systems, show their usefulness with respect to the current state of the art, and apply them to the analysis of a case study.

Three models were developed for the most common configurations of the existing pumping stations for irrigation.

The advantage of these models over the current state of the art was shown. First, the greater precision of using multipump models was shown when there are N motor pumps sharing a single PV generator. In the case of negligible hydraulic friction losses, the use of the multipump model shows gains with respect to the state of the art in which a single motor pump connected to a $1/N$ fraction of the PV generator is simulated and the result multiplied by N . However, in the case of appreciable friction losses, the current state of the art overestimates the productivity of the systems.

Second, the ability of these models to compare different multipump designs was shown. It was illustrated with the comparison of different solutions by analyzing the productivity of the three proposed configurations. The result of the comparison between subconfigurations 2.1 and 2.2 shows better performance of the second one (8% in the example used), that is, in favor of the option of two groups of pumps working at variable frequencies instead of one of the groups working at nominal frequency. In return, one of the groups operating at nominal frequency, generally the one made up of larger pumps, could present long-term reliability advantages.

Finally, the models were applied to a real PVIS in Los Monegros, Spain, which has a pumping station with two different groups of pumps. The results of simulating two different configurations (subconfigurations 2.1 and 2.2) allowed us to analyze the advantages of each one. Particularly relevant are the graphical results that allow one not only to analyze the performance but also serve as a basis for the design of the control algorithms of the real system.

These models were implemented in the free-access SISIFO simulation tool at www.sisifo.info (accessed on 8 March 2022).

This work opens the door to future lines of research for the optimization of these models. For example, the graphical tools shown in the paper could be used for:

- Better selecting the large and small pumps in each group to seek greater complementarity in order to minimize the number of pump starts/stops;
- Better withstanding fades in irradiance due to the passage of clouds;
- Better adapting to the climate of the site;
- Taking advantage of all the energy that the PV generator can produce at its maximum power point;
- Limiting the working point of the pumps to efficiency ranges close to their best efficiency point;
- Reducing the number of frequency variators required;
- Combining several of these objectives, sometimes conflicting, as long as the required pumped water flow during the irrigation period can be met.

Author Contributions: Conceptualization, J.R.L., R.H.A. and L.N.; methodology, J.R.L.; software, J.R.L.; validation, J.R.L. and R.H.A.; formal analysis, J.R.L., R.H.A. and L.N.; investigation, J.R.L., R.H.A. and L.N.; resources, J.R.L.; data curation, J.R.L.; writing—original draft preparation, J.R.L. and L.N.; writing—review and editing, J.R.L., R.H.A. and L.N.; visualization, J.R.L.; supervision, L.N.; project administration, L.N.; funding acquisition, L.N. All authors have read and agreed to the published version of the manuscript.

Funding: This work was possible thanks to the funding from the European Union's Horizon 2020 research and innovation program for the SOLAQUA project under grant agreement No. 952879 and thanks to the Project MADRID-PV2 (P2018/EMT-4308) funded by the Comunidad de Madrid with the support from ERDF Funds.

Institutional Review Board Statement: Not applicable.

Informed Consent Statement: Not applicable.

Data Availability Statement: The results can be regenerated using the SISIFO tool available online at <https://www.sisifo.info> (accessed on 27 May 2022), where some profiles are defined with the input data leading to the results presented. These profiles include in their names the label "Paper 2022/07".

Conflicts of Interest: The authors declare no conflict of interest.

Nomenclature

| | | | |
|--|--|------------------|--|
| DP | Dynamic programming | $P_{DC,B}$ | DC power at point B |
| E_1 | AC energy yield at the motor-pump input | $P_{DC,z}$ | Demanded DC power by a single pump while pumping a water flow Q_z at H_s |
| E_{DC} | DC energy yield | $P_{DC,z-1}$ | Demanded DC power of the rest of $z - 1$ active pumps, $P_{DC,z-1}$, pumping the rest of water flow, $Q_s - Q_z$ at H_s |
| $E_{DC,MPP}$ | Potential DC energy yield (at MPP) | $P_{DC,mpp}$ | Available PV power |
| E_H | Hydraulic energy yield | $P_{DC,max}$ | Maximum DC power of the equivalent pump |
| f, ω | Frequency | $P_{DC,min}$ | Minimum DC power of the equivalent pump |
| $f_{z-1}(x)$ | Cost of the rest of the path, in this case, the demanded DC power of the rest of $z - 1$ active pumps, $P_{DC,z-1}$, pumping the rest of water flow, $Q_s - Q_z$ at H_s | P_{HB} | Hydraulic power at point B |
| $g_z(x)$ | State cost function, for this case, the demanded DC power by a single pump while pumping a water flow Q_z at H_s | P_{HC} | Hydraulic power at point C |
| H | Pumping head | PV | Photovoltaic |
| H_B | Pumping head at a certain duty point not included in the $Q-H$ curve at nominal frequency | PVIS | Photovoltaic irrigation system |
| $k_{b0,1}, k_{b1,1}, k_{b2,1}$ | Parameters that fit the $Q-H$ curve of the individual pump | Q | Water flow |
| $k_{b0,N}, k_{b1,N}, k_{b2,N}$ | Parameters that fit the $Q-H$ curve of the equivalent pump of N equal pumps | Q_1 | Water flow of the individual pump |
| $k_{p0,1}, k_{p1,1}, k_{p2,1}$ | Parameters that fit the $Q-P_2$ curve of the individual pump | Q_B | Water flow at a certain duty point not included in the rated-frequency $Q-H$ curve |
| $k_{p0,N}, k_{p1,N}, k_{p2,N}$ | Parameters that fit the $Q-P_2$ curve of the equivalent pump of N equal pumps | Q_{min} | Minimum cooling water flow of the pumps |
| k_{s0}, k_{s2} | Parameters that fit the system curve | Q_N | Water flow of the equivalent pump of N pumps |
| $k_{z_n0}, k_{z_n1}, k_{z_n3}, k_{z_n4}$ | Parameters that fit the "pseudo system curves" | Q_s | Required water flow at the system curve discretized in S samples ($0 < Q_z < Q_s$) |
| m | Number of active motor pumps in the second group | $Q_{s,max}$ | Maximum required water flow at the system curve discretized in S samples |
| M | Number of motor pumps in the second group | S | Number of samples from the system curve |
| MP | Motor pump | W_{AC} | AC wiring losses |
| n | Number of active motor pumps in the first group | x | Constrained state variable |
| N | Number of motor pumps in the first group | Z | Number of equivalent pumps resulting from the possible combinations of N pumps |
| P_1 | Demanded power at the input of the motor | z | Each combination of active pumps |
| P_{1B} | P_1 at point B | η_{FC} | Frequency converter efficiency |
| P_2 | Demanded power at the pump input (1 pump) | η_{PB} | Pump efficiency at point B |
| $P_{2,N}$ | Demanded power at the pump input (N pumps) | η_{PC} | Pump efficiency at point C |
| P_{2B} | P_2 at point B | θ | Constant value that depends on the water density and gravity |
| P_{AC} | Power at the output of the frequency converter | ω_{max} | Maximum operating frequency of each individual pump |
| $P_{AC,B}$ | Power at the output of the frequency converter at point B | ω_{rated} | Rated frequency |
| P_{DC} | DC power | | |

References

- Palz, W. The French Connection: The rise of the PV water pump. *Refocus—Int. Renew. Energy Mag.* **2001**, *2*, 46–47.
- Enochian, R.V. *Solar- and Wind-Powered Irrigation Systems*; United States Department of Agriculture: Washington, DC, USA, 1982.
- Halcrow, W. *Small-Scale Solar-Powered Irrigation Pumping Systems—Technical and Economical Review*; World Bank: Washington, DC, USA, 1981.
- Barlow, R.; McNelis, B.; Derrick, A. *Solar Pumping: An Introduction and Update on the Technology, Performance, Costs, and Economics*; World Bank Technical Paper Number 168; World Bank: Washington, DC, USA, 1993.
- Fedrizzi, M.C.; Sauer, I.L. Bombeamento Solar Fotovoltaico, histórico, características e projetos. In *Encontro de Energia no Meio Rural*, 4; UNICAMP: Campinas, Brazil, 2002. Available online: http://www.proceedings.scielo.br/scielo.php?script=sci_arttext&pid=MSC000000022002000100034&lng=en&nrm=iso (accessed on 1 March 2021).
- Van Campen, B.; Guidi, D.; Best, G. *Solar Photovoltaics for Sustainable Agriculture and Rural Development*; FAO: Rome, Italy, 2000.
- Abella, M.A.; Lorenzo, E.; Chenlo, F. PV Water Pumping Systems Based on Standard Frequency Converters. *Prog. Photovolt.—Res. Appl.* **2003**, *11*, 179–191. [[CrossRef](#)]
- Ghoneim, A.A. Design optimization of photovoltaic powered water pumping systems. *Energy Convers. Manag.* **2006**, *47*, 1449–1463. [[CrossRef](#)]
- Campana, P.E.; Li, H.; Yan, J. Dynamic modelling of a PV pumping system with special consideration on water demand. *Appl. Energy* **2013**, *112*, 635–645. [[CrossRef](#)]
- Renu; Bora, B.; Prasad, B.; Sastry, O.; Kumar, K.; Bangar, M. Optimum sizing and performance modeling of Solar Photovoltaic (SPV) water pumps for different climatic conditions. *Solar Energy* **2017**, *155*, 1326–1338. [[CrossRef](#)]
- Muhsen, D.H.; Ghazali, A.B.; Khatib, T. Multiobjective differential evolution algorithm-based sizing of a standalone photovoltaic water pumping system. *Energy Convers. Manag.* **2016**, *118*, 32–43. [[CrossRef](#)]
- Bouzidi, B. New sizing method of PV water pumping systems. *Sustain. Energy Technol. Assess.* **2013**, *4*, 1–10. [[CrossRef](#)]
- Bakelli, Y.; Arab, A.H.; Azouic, B. Optimal sizing of photovoltaic pumping system with water tank storage using LPSP concept. *Sol. Energy* **2011**, *85*, 288–294. [[CrossRef](#)]
- Muhsen, D.H.; Khatib, T.; Abdulabbas, T.E. Sizing of a standalone photovoltaic water pumping system using hybrid multi-criteria decision making methods. *Solar Energy* **2018**, *159*, 1003–1015. [[CrossRef](#)]
- Olcan, C. Multi-objective analytical model for optimal sizing of stand-alone photovoltaic water pumping systems. *Energy Convers. Manag.* **2015**, *100*, 358–369. [[CrossRef](#)]
- Yahyaoui, I.; Atieh, A.; Serna, A.; Tadeo, F. Sensitivity analysis for photovoltaic water pumping systems: Energetic and economic studies. *Energy Convers. Manag.* **2017**, *135*, 402–415. [[CrossRef](#)]
- Monís, J.I.; López-Luque, R.; Reca, J.; Martínez, J. Multistage Bounded Evolutionary Algorithm to Optimize the Design of Sustainable Photovoltaic (PV) Pumping Irrigation Systems with Storage. *Sustainability* **2020**, *12*, 1026. [[CrossRef](#)]
- Suehrcke, H.; Appelbaum, J.; Reshef, B. Modelling a permanent magnet DC motor/centrifugal pump assembly in a photovoltaic energy system. *Solar Energy* **1997**, *59*, 37–42. [[CrossRef](#)]
- Hamidat, A.; Benyoucef, B. Mathematic models of photovoltaic motor-pump systems. *Renew. Energy* **2008**, *33*, 933–942. [[CrossRef](#)]
- Gherbi, A.D.; Arab, A.H.; Salhi, H. Improvement and validation of PV motor-pump model for PV pumping system performance analysis. *Solar Energy* **2017**, *144*, 310–320. [[CrossRef](#)]
- Mayer, O.; Baumeister, A.; Festl, T. Design, simulation and diagnosis of photovoltaic pumping systems with DASTPVPS. In Proceedings of the 13th European Photovoltaic Solar Energy Conference, Nice, France, 23–27 October 1995.
- Grundfos. Available online: <http://de.grundfos.com/grundfos-wincaps.html> (accessed on 4 November 2021).
- COMPASS. Available online: <https://www.lorenz.de/en/products/submersible-solar-pumps.html> (accessed on 4 November 2021).
- SOLARPACK. Available online: <http://tools.franklin-electric.com/solar/> (accessed on 4 November 2021).
- Hydraulic Calculation Tool. Available online: <http://www.netafim.com/service/hydrocalc-pro> (accessed on 4 November 2021).
- GESTAR. SETUP GESTAR. 2016. Available online: <http://www.acquanalyst.com/contenido.php?modulo=descargas&cat=2> (accessed on 4 November 2021).
- Estrada, C.; González; Aliod, R.; Paño, J. Improved pressurized pipe network hydraulic solver for applications in irrigation systems. *J. Irrig. Drain. Eng.* **2009**, *135*, 421–430. [[CrossRef](#)]
- FAO. Land & Water. Available online: http://www.fao.org/nr/water/infores_databases_cropwat.html (accessed on 4 November 2021).
- Langarita, R.; Chóliz, J.S.; Sarasa, C.; Duarte, R.; Jiménez, S. Electricity costs in irrigated agriculture: A case study for an irrigation scheme in Spain. *Renew. Sustain. Energy Rev.* **2016**, *68*, 1008–1019. [[CrossRef](#)]
- Knecht, R.; Baumgartner, F.P. PV-Battery and Diesel Hybrid System for Irrigation of a Farm in Patagonia. In Proceedings of the 33rd European Photovoltaic Solar Energy Conference and Exhibition, Amsterdam, The Netherlands, 25–29 September 2017.
- Carrêlo, I.B.; Almeida, R.H.; Narvarte, L.; Martínez-Moreno, F.; Carrasco, L.M. Comparative analysis of the economic feasibility of five large-power. *Renew. Energy* **2020**, *145*, 2671–2682. [[CrossRef](#)]
- Herraiz, J.I.; Fernández-Ramos, J.; Almeida, R.H.; Báguena, E.; Castillo-Cagigal, M.; Narvarte, L. On the tuning and performance of Stand-Alone Large-Power PV irrigation systems. *Energy Convers. Adm Manag. X* **2022**, *13*, 100175. [[CrossRef](#)]
- Almeida, R.H.; Carrêlo, I.B.; Lorenzo, E.; Narvarte, L.; Fernández-Ramos, J.; Martínez-Moreno, F.; Carrasco, L.M. Development and Test of Solutions to Enlarge the Power of PV Irrigation and Application to a 140 kW PV-Diesel Representative Case. *Energies* **2018**, *11*, 3538. [[CrossRef](#)]

34. Innovagri. El Riego Solar, una Alternativa para Rentabilizar el Consumo Energético. 2016. Available online: <https://www.innovagri.es/comunidad/el-riego-solar-una-alternativa-para-rentabilizar-la-energia.html> (accessed on 10 May 2018).
35. Energías Renovables. Powen Instala en el Campo de Albacete un Bombeo Solar para Autoconsumo de Casi Doscientos Kilovatios. 2017. Available online: <https://www.energias-renovables.com/fotovoltaica/powen-instala-en-el-campo-de-albacete-20171023> (accessed on 10 May 2018).
36. EIP Water. *European Innovation Partnership Water—Strategic Implementation Plan*; European Commission: Brussels, Belgium, 2012.
37. Ramos, J.F.; Fernandez, L.N.; de Almeida, R.H.T.; Carrêlo, I.B.; Moreno, L.M.C.; Pigueiras, E.L. Method and Control Device for Photovoltaic Pumping Systems. Spain Patent ES 2 607 253 B2, 1 March 2018.
38. Gasque, M.; González-Alltozano, P.; Gutiérrez-Colomer, R.P.; García-Marí, E. Optimisation of the distribution of power from a photovoltaic generator between two pumps working in parallel. *Solar Energy* **2020**, *198*, 324–334. [\[CrossRef\]](#)
39. Olszewski, P. Genetic optimization and experimental verification of complex parallel pumping station with centrifugal pumps. *Appl. Energy* **2016**, *178*, 527–539. [\[CrossRef\]](#)
40. Da Costa Bortoni, E.; de Almeida, R.A.; Carvalho Viana, A.N. Optimization of parallel variable-speed-driven centrifugal pumps operation. *Energy Effic.* **2008**, *1*, 167–173. [\[CrossRef\]](#)
41. Munoz, J.; Carrillo, J.; Martínez-Moreno, F.; Carrasco, L.; Narvarte, L. Modeling and simulation of large PV pumping systems. In Proceedings of the 31th European Photovoltaic Solar Energy Conference and Exhibition, Hamburg, Germany, 14–18 September 2015.
42. Bellman, R.E. *Dynamic Programming*; Princeton University Press: Princeton, NJ, USA, 1957.
43. Casti, R.L.a.J. *Principles of Dynamic Programming, Part I*; Dekker: New York, NY, USA, 1979.
44. Viholainen, J.; Tamminen, J.; Ahonen, T.; Ahola, J.; Vakkilainen, E.; Soukka, R. Energy-efficient control strategy for variable speed-driven parallel pumping systems. *Energy Effic.* **2013**, *6*, 495–509. [\[CrossRef\]](#)